Two-step production of resonant Bose-Einstein condensates

M. W. C. Sze and J. L. Bohn

Two-Step Production of Resonant Bose-Einstein Condensates

M. W. C. Sze[1], J. L. Bohn[1]

[1]*JILA and Department of Physics, University of Colorado, Boulder, Colorado 80309-0440, USA*

(Dated: February 15, 2019)

Producing a substantial and stable resonant Bose-Einstein condensate (BEC) has proven to be a challenging experimental task due to heating and three-body losses that may occur even before the gas comes to thermal equilibrium. In this paper, by considering two-body correlations, we note that a sudden quench from small to large scattering lengths is not an efficient way to prepare a resonant BEC. As an alternative, we propose a two-step scheme that involves an intermediate scattering length, between 0 and ∞, which serves to maximize the transfer probability of N bosons of mass m in a harmonic trap with frequency ω to the resonant state. We find that the intermediate scattering length should be $a \approx 3.16 N^{-2/3} \sqrt{\hbar/(m\omega)}$, and that it produces an optimum transition probability of $1.03 N^{-1/6}$.

I. INTRODUCTION

Recent experimental efforts have sought to prepare a Bose-Einstein condensate (BEC) of ultracold atoms in a regime where the two-body scattering length a is infinite [1–5]. Such a situation is termed a "resonant" (or sometimes "unitary") BEC. It represents a special situation, inasmuch as the perturbative parameter na^3 – where n is the number density – is no longer small and the usual field-theoretic treatments would require evaluation to very high orders of perturbation theory. This circumstance has led to a variety of alternative theoretical descriptions, which are in general agreement about the nature of the gas, yet differ in details [6–18].

On the experimental side, producing the resonant BEC is problematic, since the rate of three-body recombination grows rapidly with scattering length. In the resonant limit, this rate ultimately saturates, but at a large value that ensures the heating and ultimate destruction of the gas within milliseconds. Under these circumstances, a semblance of the approach to equilibrium can be teased out [3, 4, 19], while the loss can be understood as a few-body process incorporating local physics of the gas [17, 20–22].

In order to perform an experiment of this kind at all, the resonant BEC must therefore be produced quickly. A typical experimental protocol starts with the gas at a small value of scattering length, then rapidly ramps the value of a magnetic field near a Fano-Feshbach resonance so that $a \to \infty$ within microseconds. This represents the essentially instantaneous projection of the many-body state at small a onto a collection of many-body states at $a = \infty$.

The sudden projection may not be the optimal way to produce the resonant BEC. To see this, at least qualitatively, it is useful to regard the gas within a mean-field-like description. Consider a gas of N identical bosons, each initially in some single-particle orbital $\phi_a(\mathbf{r})$, corresponding to the small initial scattering length a (the function ϕ_a could be the ground state solution to the Hartree-Fock equations for the Bose system, for example). The many-body wave function is then, to a good approximation,

$$\Psi(\mathbf{r}_1, \mathbf{r}_2, \dots \mathbf{r}_N) = \prod_{i=1}^{N} \phi_a(\mathbf{r}_i). \tag{1}$$

Similarly, on resonance each atom can be regarded as belonging to some different orbital wave function $\psi_\infty(\mathbf{r})$. This could be obtained approximately, for example, by performing a Hartree-Fock calculation using a renormalized scattering length $a \propto n^{-1/3}$ [6–10, 23]. Thus, at least up to a certain approximation, the desired resonant BEC is described by

$$\Psi_{\text{res}}(\mathbf{r}_1, \mathbf{r}_2, \dots \mathbf{r}_N) = \prod_{i=1}^{N} \psi_\infty(\mathbf{r}_i). \tag{2}$$

Then the probability that all the atoms in the initial state Ψ are transferred to the resonant BEC states Ψ_{res}, assuming that the fast ramp results in a projection, is given by the square of their overlap

$$P = |\langle \Psi | \Psi_{\text{res}} \rangle|^2 = \left(\left| \int d^3 r \phi_a^*(\mathbf{r}) \psi_\infty(\mathbf{r}) \right|^2 \right)^N \tag{3}$$

Unless each of these overlap integrals is very close to one, the product of N of them will be vanishingly small for typical experimental circumstances with $N > 10^3$. For this reason, it appears that, while the sudden ramp to $a = \infty$ produces an interesting, nonequilibrium gas of strongly-interacting bosons, it is unlikely to generate the desired resonant BEC.

In this paper we present an alternative scheme for preparing a resonant BEC, which proceeds in two steps. In a first step, the scattering length is jumped quickly from a low initial value $a \approx 0$ to a modest intermediate value a^*. The sudden increase in scattering length causes the BEC to expand; when it reaches the size of the resonant BEC, the scattering length is suddenly jumped from a^* to $a = \infty$. For a properly-chosen value of the intermediate scattering length a^*, we show that the fraction of atoms converted into a resonant BEC can be non-negligible [24].

To describe and carry out calculations of this scheme, we focus on an isotropic, harmonically trapped BEC and

employ a coordinate-based representation of the BEC wave function. This representation presents the BEC as a wave packet subject to an effective potential energy surface (PES) [25], and it has recently been shown to make a reasonable description of the BEC on resonance [9, 10]. It presents the dynamics as the time evolution of a wave packet obeying a linear Schrödinger equation. In these terms the two-step process is reminiscent of vibrational wave packet dynamics in molecular physics [26]. It is also amenable to analytic approximations, which will yield simple estimates for the optimum value of the intermediate scattering length a_2, as well as the approximate yield of atoms in the resonant BEC at the end of the two steps.

II. POTENTIAL ENERGY SURFACES, QUENCH FROM NON-INTERACTING TO RESONANT BEC'S

The theoretical machinery that we employ to construct approximate BEC wave functions is detailed in Ref. [10]. Here we summarize the highlights of the theory to provide context for the results that follow. For further details we refer the reader to Ref. [10].

We consider a system of N bosonic atoms confined in a spherically symmetric harmonic oscillator potential with angular frequency ω. Because of the diluteness of the system under typical experimental conditions, we model the system as described by particles with coordinates $\mathbf{r}_i$ governed by a harmonic oscillator Hamiltonian

$$H = \sum_{i=1}^{N} \left(\frac{p_i^2}{2m} + \frac{1}{2} m\omega^2 r_i^2 \right), \qquad (4)$$

with two-body interactions represented by the zero-range two-body boundary conditions, given by the Bethe-Peierls condition

$$\lim_{r_{ij} \to 0} \frac{1}{r_{ij}\psi} \frac{\partial(r_{ij}\psi)}{\partial r_{ij}} = -\frac{1}{a}, \qquad (5)$$

where a is the two-body scattering length and $r_{ij} = |\mathbf{r}_i - \mathbf{r}_j|$. After removing the center of mass, the relative coordinates of the particles are conveniently described by mass-weighted Jacobi coordinates defined by

$$\boldsymbol{\eta}_k = \sqrt{\frac{N-k}{N-k+1}} \left(\mathbf{r}_{N-k+1} - \frac{1}{N-k} \sum_{j=1}^{N-k} \mathbf{r}_j \right). \quad (6)$$

The Jacobi coordinates define Cartesian coordinates in a $3(N-1)$-dimensional configuration space.

We exploit a coordinate representation of BEC that is expressed in terms of potential energy surfaces (PES's) analogous to Born-Oppenheimer (B.-O.) curves in molecular physics. To do so, we define a single, collective coordinate, the hyperradius ρ, which represents the size of the condensate [27]:

$$\rho^2 = \sum_{k=1}^{N-1} \eta_k^2 = \frac{1}{N} \sum_{i<j}^{N} r_{ij}^2. \qquad (7)$$

All remaining coordinates, collectively denoted by Ω, span a hypersphere of radius ρ in a $(3N-4)$-dimensional configuration space. They are conveniently parametrized by a set of angles, including the directions of the unit vectors $\hat{\boldsymbol{\eta}}_k$, along with the radial correlation angles α_k defined by

$$\sin \alpha_k = \frac{\eta_k}{\left(\sum_{l=1}^{k} \eta_k^2 \right)^{1/2}}. \qquad (8)$$

In these coordinates the Hamiltonian is given by [27]

$$H_{\rm rel} = -\frac{\hbar^2}{2m} \left[\frac{1}{\rho^{3N-4}} \frac{\partial}{\partial \rho} \rho^{3N-4} \frac{\partial}{\partial \rho} - \frac{\Lambda_{N-1}^2}{\rho^2} \right] + \frac{1}{2} m\omega^2 \rho^2, \qquad (9)$$

where m is the atomic mass and ω is the angular frequency of the isotropic harmonic trap. Thus the kinetic energy has a radial part and an angular part, the latter given in general by the grand angular momentum Λ_{N-1}^2, a differential operator that can be defined recursively [27],

$$\Lambda_k^2 = \Pi_k^2 + \frac{\Lambda_{k-1}^2}{\cos^2 \alpha_k} + \frac{l_k^2}{\sin^2 \alpha_k}, \quad k = 2, 3, ..., N-1 \quad (10)$$

with

$$\Pi_k^2 = -\frac{\partial^2}{\partial \alpha_k^2} + \frac{(3k-6) - (3k-2)\cos(2\alpha_k)}{\sin(2\alpha_k)} \frac{\partial}{\partial \alpha_k}, \quad (11)$$

$\{0 \leq \alpha_k \leq \pi/2\}$, and l_k is the orbital angular momentum of the vector $\boldsymbol{\eta}_k$ which we choose to be zero. In particular the hyperangular coordinate $\alpha = \alpha_{N-1}$, given by $\sin \alpha = r_{12}/\left(\sqrt{2}\rho\right)$ incorporates the two-body coordinate between atoms 1 and 2. In some treatments in the literature, the authors have attempted to incorporate realistic two-body interaction potentials for rubidium atoms in this coordinate [28–31]. Others [27, 32–34] have adopted a zero-range approximation for two-body interactions, replacing the interaction potential with the Bethe-Peierls boundary conditions. We adopt the latter approach here.

Under the B.-O. approximation, the hyperradius ρ is treated as the slow coordinate. That is, at each value of ρ, the Schrödinger equation, is solved in the hyperangular coordinates Ω to yield a set of ρ-dependent eigenenergies of the operator $\frac{\hbar^2}{2m\rho}\Lambda_{N-1}^2$, along with the corresponding eigenfunctions $Y_{\{\lambda\}}(\rho; \Omega)$. Taken as a function of ρ, these energies constitute a set of adiabatic potential energy curves $V_{\{\lambda\}}(\rho)$ for the motion in ρ. Here $\{\lambda\}$ denotes a set of quantum numbers required to specify the wave function in all coordiantes of Ω. A coupled set of differential equations is obtained if we expand the wave function

Ψ in adiabatic hyperangular basis,

$$\Psi = \rho^{-(3N-4)/2} \sum_{\{\lambda\}} F_{\{\lambda\}}(\rho) Y_{\{\lambda\}}(\rho; \Omega), \qquad (12)$$

for some set of radial expansion functions $F_{\{\lambda\}}$. The eigenfunctions $Y_{\{\lambda\}}(\rho; \Omega)$ are eigenfunctions of the $3N-4$-dimensional partial differential operator Λ_{N-1}^2. In practice, we find approximate eigenfunctions by invoking the Jastrow approximation, which factors the total wave function into a product of pair wave functions of the form

$$Y_\nu = \frac{\prod_{i<j} \phi_\nu(\rho; \alpha_{ij})}{\sqrt{\int d\Omega \prod_{i<j} \phi_\nu(\rho; \alpha_{ij})^2}}. \qquad (13)$$

Within this approximation, each two-body function $\phi_\nu(\alpha)$ satisfies an ordinary partial differential equation that is detailed in Ref.[10], subject to the Bethe-Peierls boundary condition, which in this coordinate system and at fixed ρ takes the form

$$\lim_{\alpha \to 0} \frac{1}{\sqrt{2}\rho(\alpha\phi_\nu)} \frac{\partial(\alpha\phi_\nu)}{\partial\alpha} = -\frac{1}{a}. \qquad (14)$$

By using this *ansatz*, each ϕ_ν solves an ordinary differential equation and requires only a single quantum number ν, which replaces the set of $3N-4$ quantum numbers $\{\lambda\}$. We will continue to use this notation in what follows.

Within the B.-O. approximation the hyperradial motion is independent within each channel ν. This has been justified by experience in the case of the relatively small scattering lengths that are found in non-resonant BEC experiments [25, 34]. Moreover, the B.-O. approximation has been shown to be exact on resonance, at least when considering only two-body interactions, as we do here [36, 37]. We will employ this approximation throughout, writing the wave function as

$$\Psi = \rho^{-(3N-4)/2} F_\nu(\rho) Y_\nu(\rho; \alpha) \qquad (15)$$

for the channel with the lowest value of ν, representing the ground state of relative excitation. The ground state of $V_\nu(\rho)$ represents the BEC ground state, and excitations in ρ represent breathing modes of the condensate.

Using a single adiabatic function, the Schrödinger equation becomes a single ordinary differential equation in ρ:

$$\left[-\frac{\hbar^2}{2m} \frac{d^2}{d\rho^2} + V^{\mathrm{diag}}(\rho) + V_\nu(\rho) \right] F_\nu(\rho) = E_{\mathrm{rel}} F_\nu(\rho), \qquad (16)$$

where

$$V^{\mathrm{diag}}(\rho) = \frac{\hbar^2}{2m} \frac{(3N-4)(3N-6)}{4\rho^2} + \frac{1}{2} m\omega^2 \rho^2, \qquad (17)$$

$$V_\nu(\rho) = \frac{\hbar^2}{2m\rho^2} \langle\nu|\Lambda_{N-1}^2|\nu\rangle. \qquad (18)$$

V^{diag} is the diagonal potential whose ground state supports the non-interacting condensate wave function. V_ν represents the contribution due to interactions, namely, the eigenenergy of Λ_{N-1}^2 as determined above. It is a function of both the hyperradius and the scattering length. Calculation of the matrix element $\langle\nu|\Lambda_{N-1}^2|\nu\rangle$, which involves integration over the entire hypersphere, is not trivial. In this paper, we use the results of Ref. [10], where a lowest-order constraint variational approximation has been applied to obtain a meaningful outcome even for $a = \infty$. In general V_ν must be determined numerically, but Ref. [10] derives useful approximations to this potential in the very small and very large-a limits, which we will employ in the following. Thus, for any scattering length a, we find a B.-O. potential

$$V^a(\rho) = V^{\mathrm{diag}}(\rho) + V_\nu(\rho). \qquad (19)$$

We will denote the associated hyperangular wave function by $\Phi^a(\rho; \Omega)$, to make explicit the scattering length for which this function was calculated. Here the notation ν is suppressed, since it is understood we are considering the lowest value of ν. Vibrational states in the PES $V^a(\rho)$ constitute the radial wave functions $F_n^a(\rho)$, each vibration n describing a breathing mode excited above the ground state condensate with $n = 0$. The states relevant to our model are, therefore, defined by the scattering length a and the number of breathing quanta,

$$|a, n\rangle = \rho^{-(3N-4)/2} F_n^a(\rho) \Phi^a(\rho; \Omega). \qquad (20)$$
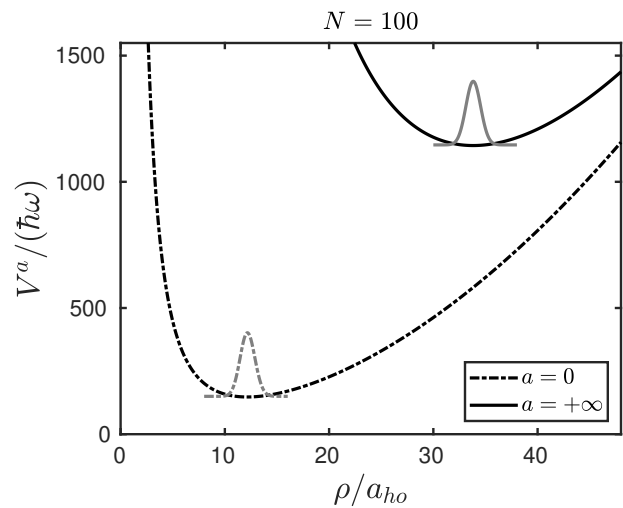

FIG. 1. The scale of the problem. Each curve represents an effective potential energy surface for a BEC with $a = 0$ (bottom) and $a = \infty$ (top), in our hyperspherical representation. A BEC having $a = 0$ (Gaussian centered at $\rho = 12.2\, a_{ho}$) has essentially no overlap with a resonant BEC having $a = \infty$ (Gaussian centered at $\rho = 33.8\, a_{ho}$).

Figure 1 shows the B.-O. PES's for the non-interacting ($a = 0$) and resonant ($a = \infty$) cases for a gas of $N = 100$

atoms. With $a = 0$, $V^0(\rho) = V^{\text{diag}}(\rho)$. This PES, the lowest curve on the left, is exact. Its minimum value occurs at

$$\rho^0 \underset{N \gg 3}{\approx} \sqrt{\tfrac{3N}{2}} a_{ho}, \qquad (21)$$

where $a_{ho} = \sqrt{\hbar/(m\omega)}$. The topmost curve on the right is an approximate surface for the resonant limit. In the large N limit, this potential is given by

$$V^\infty(\rho) = \frac{\hbar^2}{2m\rho^2}\left(\frac{9N^2}{4} + 3c_0 N^{8/3}\right) + \frac{1}{2}m\omega^2\rho^2, \quad (22)$$

where $c_0 \approx 2.122$ is a constant determined from $c_0 = x_0^2/(16\pi)^{1/3}$ and x_0 is the smallest root of the transcendental equation $1 + x_0 \tan x_0 = 0$. This result is derived in Appendix C of Ref. [10]. For realistic values of $N > 10^2$, the centrifugal term with $9N^2/4$ can be safely neglected. Then the minimum of V^∞ is located near

$$\rho^\infty \underset{N \gg 3}{\approx} (3c_0)^{1/4} N^{2/3} a_{ho}. \qquad (23)$$

Near their minima, we approximate these potentials as harmonic oscillators:

$$V^0(\rho) \approx \frac{3N}{2}\hbar\omega + \frac{1}{2}m(2\omega)^2(\rho - \rho^0)^2, \qquad (24)$$

$$V^\infty(\rho) \approx (3c_0)^{1/2} N^{4/3} + \frac{1}{2}m(2\omega)^2(\rho - \rho^\infty)^2. \qquad (25)$$

In both cases, the excitation frequency of the radial breathing modes considered is exactly twice the trap frequency, $\omega_b = 2\omega$. For non-interacting bosons, the energies are well-known and are given by [35]

$$E_{n,K} = \hbar\omega\left(2n + K + \frac{3N-3}{2}\right), \qquad n = 0,1,2,... \qquad (26)$$

and $K = 0,1,2,...$ is the quantum number associated with the hyperangular component. For the resonant gas, the 2ω frequency was anticipated by symmetry considerations in Refs. [36, 37]. Without considering three-body or higher order correlations, these references also emphasize that the B.-O. approximation is exact in the $a = \infty$ limit. Corrections beyond the B.-O. approximation arise because the adiabatic wave functions Φ change from one value of ρ to the next. But this change is only effective if ρ changes significantly on the scale of a, i.e., the corrections are of order ρ/a and vanish in the infinite scattering length limit. Therefore, if the atoms could be prepared in the state $F^\infty \Phi^\infty$ that we describe, this state would be stable against non-adiabatic transitions to whatever other states there are that could lead to heating, loss, etc. This stability is reduced if we were to include explicit three-body correlations in the wave function.

From the harmonic oscillator nature of the potential curves in Eqs. (24) and (25), the expected ground state hyperradial wave functions are Gaussians centered at the minima and with root-mean-squared width of $a_{ho}/\sqrt{2}$:

$$F^0(\rho) = \left(\frac{2}{a_{ho}^2 \pi}\right)^{1/4} \exp[-(\rho - \rho^0)^2/a_{ho}^2], \qquad (27)$$

$$F^\infty(\rho) = \left(\frac{2}{a_{ho}^2 \pi}\right)^{1/4} \exp[-(\rho - \rho^\infty)^2/a_{ho}^2], \qquad (28)$$

The unnormalized Gaussian functions F^0 and F^∞ for $N = 100$ are illustrated as Gaussian-shaped humps at the bottom of the $a = 0$ and $a = \infty$ PES's, respectively, in Fig. 1. From this picture, we see that the centers are far away from each other such that quenching the gas suddenly from $a = 0$ to $a = \infty$ will yield a low transfer probability. That is, the probability of the atoms landing in the resonant BEC state F^∞, upon a direct quench, is

$$|\langle 0,0,|\infty,0\rangle|^2 = \left|\int d\rho F^0(\rho) F^\infty(\rho)\right|^2 \left|\int d\Omega \Phi^0(\Omega)\Phi^\infty(\Omega)\right|^2$$
$$\leq \left|\int d\rho F^0(\rho) F^\infty(\rho)\right|^2 \approx \exp\left(-1.3N^{4/3}\right), \qquad (29)$$

which is negligible for large N.

III. THE TWO-STEP SCHEME
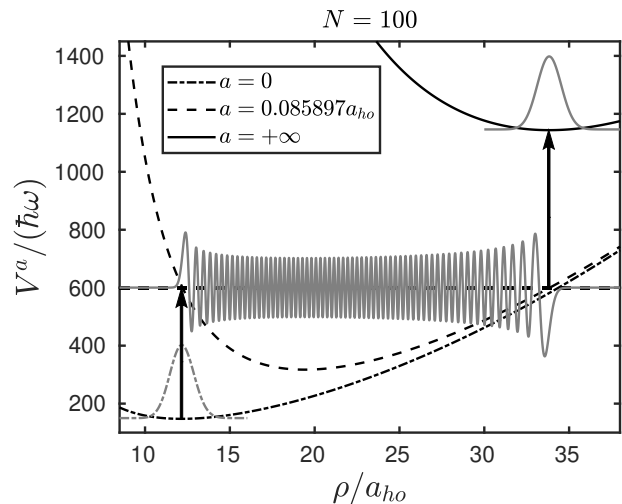
A. Franck-Condon Factors

FIG. 2. The two-step scheme from non-interaction to small a then to resonance.

The miniscule overlap between the non-interacting and resonant wave functions F^0 and F^∞ suggests that direct projection from $a = 0$ to $a = \infty$ will not yield a resonant BEC. As an alternative, we propose a two-step scheme, in which we identify an intermediate scattering length a and its Born-Oppenheimer curve $V^a(\rho)$. Such a PES is shown as the intermediate curve in Fig. 2. A good candidate for

$V^a(\rho)$ is one that supports a set of vibrational excitations n such that the Franck-Condon factors $|\langle 0,0|a,n\rangle|^2$ and $|\langle a,n|\infty,0\rangle|^2$ describe a maximum transfer probability to the resonant BEC. This idea is illustrated in Fig. 2 for $N = 100$ atoms.

Numerically calculated Franck-Condon (FC) factors are shown as color-map plots in Fig. 3 for $N = 100$; the x-axis is the scattering length, y-axis the vibrational state n, and the color indicates the transition probability. In general, for the first step from the non-interacting state to the intermediate state, the optimum transition occurs when a is small and for low n states, decreasing quickly with increasing a and n as shown in Fig. 3(a). For the second step from the intermediate state to the final state, the transition is optimum when a and n are larger, and diminishes slowly with decreasing a and increasing n as in Fig. 3(b). These two steps cannot be individually at their maxima under the same conditions. However, the best overall yield, given by the product of the FC factors, occurs when a is still small relative to the oscillator length and for higher vibrational states. This is true for any large values of N. Further, the two-step transition probabilities seem to decrease as a function of N. See the transition probability for $N = 1000$ in Fig. 4.

B. The Optimum Intermediate State

Since the intermediate state will have a small value of a, we can use a perturbative approximate expression for V^a. In the limits of perturbative $a \ll a_{ho}$ and large N, this is given by (see Appendix B of Ref. [10])

$$V^a(\rho) \underset{N \gg 3}{\approx} V^0(\rho) + \frac{\hbar^2}{m} d_0 N^{7/2} \frac{a}{\rho^3}, \tag{30}$$

where $d_0 = (3/4)\sqrt{3/\pi} \approx 0.733$. Because of the oscillatory nature of the intermediate radial wave functions $F_n^a(\rho)$, the FC factors are largest when the inner and outer turning points of V^a – denoted by ρ_{1n} and ρ_{2n}, respectively, – coincide with the minima ρ^0 and ρ^∞ of the initial and final states, a scenario suggested in Figure 2. We will make this idea more precise in what follows, but this observation enables us to approximately determine the optimum intermediate scattering length, a^*, that maximizes the product of FC factors.

Assume the intermediate state of potential V^a has energy E_a. Then its inner classical turning point is determined by $V^a(\rho_{1n}) = E_n$. For small ρ, V^a is well-approximated by the interaction term in Eq. (30) alone, whereby this criterion becomes

$$V^a(\rho_{1n}) = E_n^a \underset{N \gg 3}{\approx} \frac{\hbar^2}{m} d_0 N^{7/2} \frac{a}{\rho_{1n}^3}. \tag{31}$$

Likewise, near the outer classical turning point of V^a, this potential is well-approximated by the harmonic oscillator potential, and so

$$V^a(\rho_{2n}) = E_n^a \approx \frac{1}{2} m \omega^2 \rho_{2n}^2. \tag{32}$$

Setting $\rho_{1n} = \rho^0$ and $\rho_{2n} = \rho^\infty$ and using (21) and (23), we can solve for the optimal values of scattering length and intermediate energy:

$$a^* \underset{N \gg 3}{\approx} \frac{1}{2d_0} \left(\rho^0\right)^3 \left(\rho^\infty\right)^2 N^{-7/2} \frac{1}{a_{ho}^4} \tag{33}$$

$$E^* \approx \frac{1}{2} \left(\frac{\rho^\infty}{a_{ho}}\right)^2 \hbar\omega. \tag{34}$$

Using these approximations for $N = 100$, the results are $a^* = 0.145 a_{ho}$ and $E^* = 571.2\hbar\omega$, and are comparable to the values $a^* = 0.0859 a_{ho}$ and $E^* = 598.9\hbar\omega$, determined by numerically maximizing the FC factors. Expressions (33) and (34) become better estimates for larger N. For $N = 1000$, they yield $a^* = 0.0316 a_{ho}$ and $E^* = 1.26 \times 10^4 \hbar\omega$, whereas the numerically optimized values are $a^* = 0.0332 a_{ho}$ and $E^* = 1.28 \times 10^4 \hbar\omega$.

C. Wave Packet Dynamics

While this static picture provides an overall motivation for the two-step procedure, it does not describe the dynamics involved. Roughly, upon the initial projection from $a = 0$ to the intermediate value a^*, a wave packet is formed at ρ_{1n}. In approximately one half of the trap period, this wave packet propagates to ρ_{2n}, giving the condensate its maximum radial extent and preparing it for projection onto the resonant BEC state.

With a given intermediate potential V^a, we describe the time dynamics of the BEC by expressing the initial state after the first step as a wave packet expanded in the basis of the vibrational states of V^a

$$\begin{aligned}|\Psi^a(t)\rangle &= \sum_{n=0}^{\infty} |a,n\rangle\langle a,n|\Psi^a(t=0)\rangle e^{-iE_n t/\hbar}\\ &= \sum_{n=0}^{\infty} |a,n\rangle\langle a,n|0,0\rangle e^{-iE_n t/\hbar},\end{aligned} \tag{35}$$

where at time $t = 0$, Ψ^a is at the ground state of the non-interacting potential with total energy $E \approx 3N\hbar\omega/2$. The probability of projecting the wave packet onto the desired resonant BEC ground state is given by

$$P(t) = |\langle \infty, 0|\Psi^a(t)\rangle|^2, \tag{36}$$

where

$$\langle \infty, 0|\Psi^a(t)\rangle = \sum_{n=0}^{\infty} \langle \infty, 0|a,n\rangle\langle a,n|0,0\rangle e^{-iE_n t/\hbar}. \tag{37}$$

We first extract numerically the most appropriate choice for the intermediate scattering length, a^*, by maximizing the product of the FC factors. We then compute the transition probability at different times with
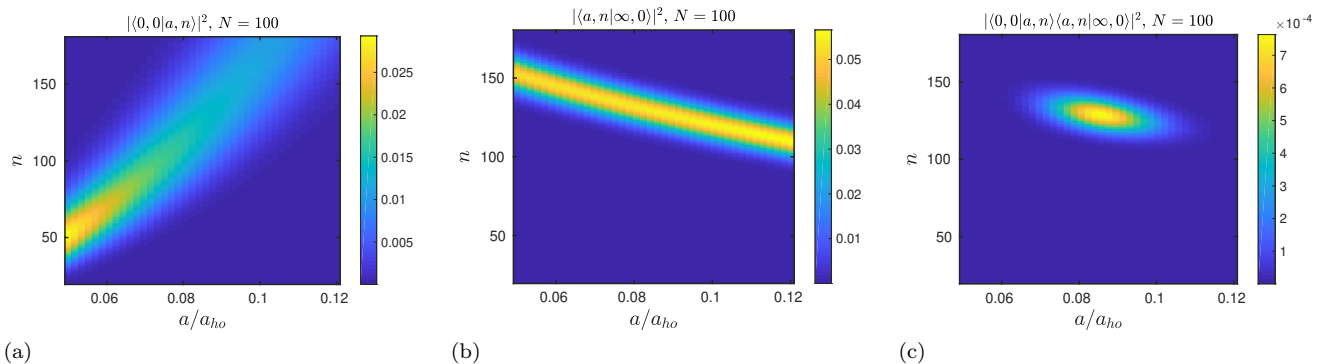
FIG. 3. Franck-Condon factors from the (a) non-interacting to intermediate states $|\langle 0,0|a,n\rangle|^2$, (b) intermediate to resonant states $|\langle a,n|\infty,0\rangle|^2$, and (c) the two-step transition probability $|\langle 0,0|a,n\rangle\langle a,n|\infty,0\rangle|^2$ as functions of scattering lengths a and vibrational states n. Here, $N=100$.
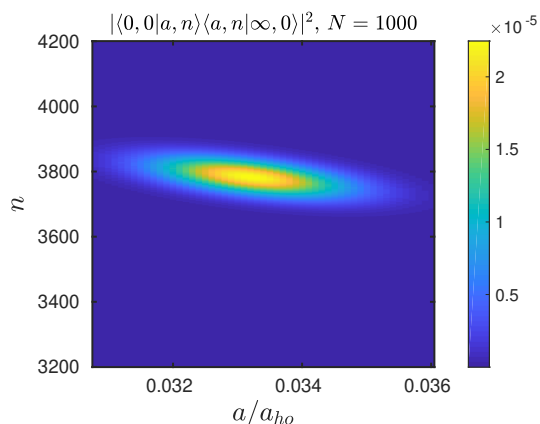

FIG. 4. The two-step transition probability distribution $|\langle 0,0|a,n\rangle\langle a,n|\infty,0\rangle|^2$ as a function of scattering lengths a and vibrational states n for $N=1000$.

the unitary BEC model found in Ref.[10] for $N=100$ and $N=1000$. Figures 5(a) and (b) show that the first maximum transition occurring at around $t_m \approx \pi/(2\omega)$. It takes about half a period, $T/2$, for the BEC to expand to resonance starting from the left side of the V^a; the breathing mode frequency is close to 2ω, thus the dwell time is $t_m \approx T/2 = \pi/\omega_b = \pi/(2\omega)$. Most importantly, the transfer probability is significant: it is 48% for $N=100$ and 37% for $N=1000$. This is a far better yield in the resonant state that the direct projection result in Eq. (29).

Figure 6 shows how the size of the BEC with $N=100$ atoms, expressed in terms of the mean hyperradius $\langle\rho\rangle$, is changing over time. It starts with $\rho=\rho^0$, the size of the non-interacting gas, and reaches $\rho=\rho^\infty$, the size of the resonant BEC, at $t\approx t_m$. The peaks of $P(t)$ and $\langle\rho\rangle$ decrease slowly over time as the wave packet gradually dephases. It is, therefore, worthwhile to instigate the second projection, to resonance, at time $t=T/2$.
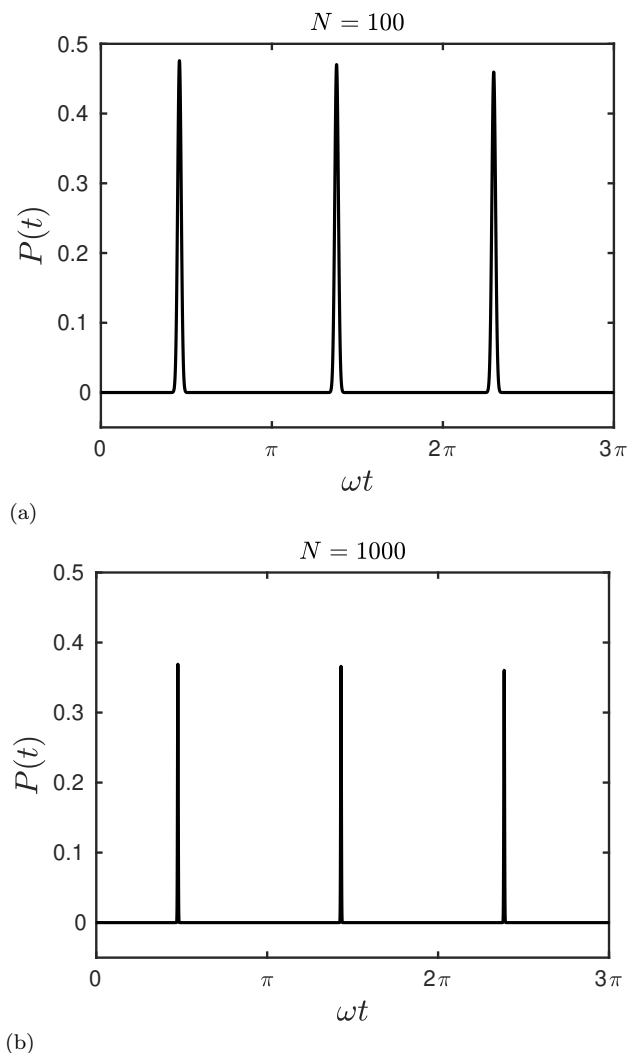

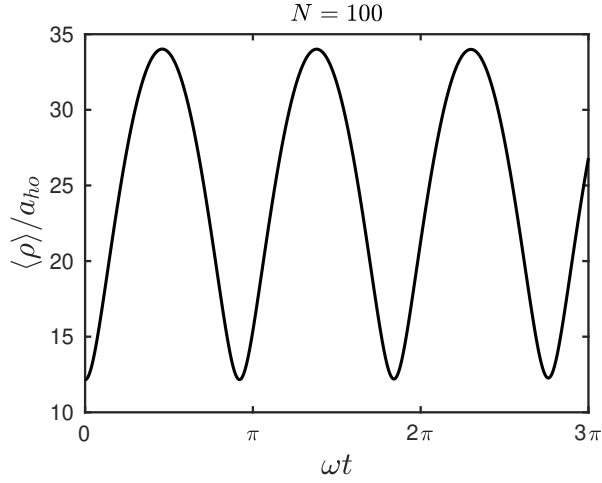FIG. 5. Transfer probability for (a) $N=100$ with $a^*=0.0859a_{ho}$, and (b) $N=1000$ with $a^*=0.0332a_{ho}$.

FIG. 6. Mean radius of the BEC in the intermediate phase versus time before quench to unitarity for $N = 100$ and $a = 0.0859a_{ho}$.

IV. LARGE N LIMIT

In calculating the $P(t)$ numerically, we notice that $P(t_m)$ decreases with N. Determining how $P(t_m)$ scales with N is extremely useful. Here, we outline a method to get a good estimate for this scaling. The details are found in the Appendix, and the final result turns out to be simple.

Using the results from Appendix A and B, the overlap integrals in Eq. (37) are approximated to be

$$\langle a, n|0, 0\rangle = \langle F_n^a|F^0\rangle_\rho \langle \Phi^a|\Phi^0\rangle_\Omega$$
$$\approx F^0(\rho_{1n})\sqrt{\frac{dE_n}{dn}}\sqrt{\frac{1}{|\partial V^a/\partial\rho|_{\rho_{1n}}}}, \quad (38)$$

$$\langle \infty, 0|a, n\rangle = \langle F^\infty|F_n^a\rangle_\rho \langle \Phi^\infty|\Phi^a\rangle_\Omega$$
$$\approx (-1)^n F^\infty(\rho_{2n})\sqrt{\frac{dE_n}{dn}}\sqrt{\frac{1}{|\partial V^a/\partial\rho|_{\rho_{2n}}}}, \quad (39)$$

where dn/dE_n is the density of vibrational states in the intermediate potential. For the hyperangular parts of the wave function we approximate

$$\langle \Phi^a|\Phi^0\rangle_\Omega \approx 1 - \frac{2}{\pi^3}\left(\frac{a}{\rho_{1n}}\right)^2\left(\frac{\pi}{6}\right)^{1/6} N^{-5/6} \approx 1, \quad (40)$$

$$\langle \Phi^\infty|\Phi^a\rangle_\Omega \approx 1 - 0.151N^{-5/2} \approx 1, \quad (41)$$

since N is large and a/ρ_{1n} is small.

Next, we convert the discrete sum in Eq. (37) into a continuum integral over the energy and evaluate it at $t = t_m$ around which the maximum transfer occurs. See Appendix C for details. The resulting transition amplitude is

$$\langle \infty, 0|\Psi^a(t_m)\rangle \approx \frac{2(2d_0)^{1/6}}{(3c_0)^{5/24}\sqrt{3}}N^{1/36}\left(\frac{a}{a_{ho}}\right)^{1/6}\exp\left[-\left(\left(\frac{2d_0}{\sqrt{3c_0}}\right)^{1/3}N^{13/18}\left(\frac{a}{a_{ho}}\right)^{1/3} - \sqrt{\frac{3N}{2}}\right)^2\right], \quad (42)$$

where c_0 and d_0 are defined in Eqs. (22) and (30). Plots of $P(t_m)$, calculated in this way, for different N are shown in Fig. 7 as a function of the intermediate scattering length a. We see that the estimated maximum transfer for $N = 10^3$ is $\sim 33\%$, which is close to what the exact calculation gives. The inset in Fig. 7 shows the sensitivity of the transition probability to the intermediate a for $N = 10^5$. The intermediate a should at least be within 0.4% from the optimum to get at least half of the maximum transfer. By maximizing Eq. (42) with respect to a, the optimum scattering length a^* is found to be

$$a^* = (3/2)^{3/2}\sqrt{3c_0}/(2d_0)N^{-2/3}a_{ho} \approx 3.16N^{-2/3}a_{ho}, \quad (43)$$

which matches the a^* obtained in Eq. (33) using Eqs. (21) and (23). And the maximum transfer is

$$\max\left(|\langle \infty, 0|\Psi^a(t_m)\rangle|^2\right) \approx \left|\left(\frac{8}{3}\right)^{1/4}\frac{1}{(3c_0)^{1/8}}N^{-1/12}\right|^2$$
$$\approx 1.028N^{-1/6}. \quad (44)$$

To put this into context, for ^{85}Rb in a trap with frequency $\omega = 2\pi \times 10\,\text{Hz}$, the oscillator length is $a_{ho} = 6.51 \times 10^4\,a_0$. Starting with $N = 10^5$ non-interacting atoms in the trap, the two-step process would be optimized for a scattering length of $a^* \approx 95.4\,a_0$ with a theoretical transfer probability of 15%.

The yield into the final state actually goes down as the number of atoms increases. Qualitatively, this is because the range of hyperradius, from, ρ^0 to ρ^∞, increases as N grows, thus the wave packet broadens more during propagation, and its overlap with the target wave function is reduced.

Finally, it is worth considering the effect of starting from a non-zero initial scattering length. Some numer-
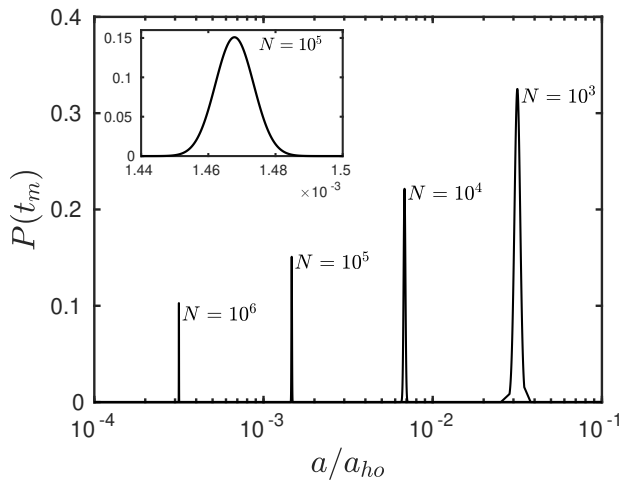
FIG. 7. Transfer probability of the BEC versus scattering length a for large N. Inset shows a zoom-in profile of $N = 10^5$.

ical experimentation finds that this would not produce a large effect. As an example, consider $N = 1000$ ^{85}Rb atoms in a spherically symmetric trap with frequency $\omega = 2\pi \times 10$ Hz. Within the model where the initial scattering length $a = 0$, numerical optimization of the transfer probability yields a 37% probability, passing through an intermediate state, via scattering length $2200a_0$. By contrast, starting with a more realistic scattering length for a stable, mean-field BEC, for example $a = 142a_0$, raises the final transfer probability only to 39%, while changing the intermediate scattering length to $2700a_0$. For greater numbers of atoms, the intermediate scattering length a^* is reduced. Since the initial scattering length must be smaller than the intermediate scattering length, regarding the initial scattering length as small becomes increasingly justified. Hence the yield in the resonant BEC is well-approximated by the $a = 0$ initial state considered.

V. CONCLUSIONS AND PROSPECTS

We have presented a protocol designed to implant a nontrivial fraction of the trapped atoms into a resonant BEC. It remains to be understood what the consequences of this preparation step will be. It is not clear, for example, how the non-equilibrium gas produced in the two-step method will begin to come to equilibrium, and whether this process is different from the case of a direct quench to resonance. It is equally unclear at present how three-body losses would differ in the resonant BEC thus produced than in a gas of equivalent density. A useful

initial experiment might be to prepare the resonant BEC as proposed here, and compare its dynamics to that of a gas of equal initial density as the resonant BEC, but jumped suddenly to resonance.

This experiment would unfortunately be clouded by another issue. Consider, for example, that starting from a non-interacting BEC of $N = 10^4$ atoms, our protocol is expected to transfer only one fifth of them to the resonant BEC. What becomes of the rest? They are presumably projected onto other quantum mechanical states of the system, each of which has its own dynamics and three-body loss rates. To address this, it is necessary to formulate a reliable theory of excited states, in our case in the hyperangular degrees of freedom. This pursuit is currently underway.

ACKNOWLEDGMENTS

Appendix A: Franck-Condon Factors Using the Reflection Formula

Here, we evaluate overlap integrals

$$\langle F_n^a | F^0 \rangle_\rho = \int_0^\infty d\rho\, F_n^a F^0, \tag{A1}$$

$$\langle F^\infty | F_n^a \rangle_\rho = \int_0^\infty d\rho\, F^\infty F_n^a. \tag{A2}$$

Leading contribution to the Franck-Condon factors comes from the overlap of wave functions at the classical turning points, where the wave functions F_n^a are sharply peaked. In between the turning points, the wave functions are highly-oscillating. Yet, we can consider that the projections of F_n^a to F^0 and F^a are still localized to the turning points since the latter wave functions are also localized (or close to zero where F_n^a is wildly oscillating). The idea that the Franck-Condon factors can be estimated from properties of the potential near the turning points is not novel [38, 39]. It is widely used in theories of optical and Raman transitions in molecules, and recently to photoassociation of cold atoms as well [40–44]. Out of these types of molecular spectroscopy studies, the reflection formula was developed [44, 45], which we will adapt.

We first express F_n^a in terms of the energy-normalized wavefunction F_E through

$$\langle F_n^a | F_{n'}^a \rangle = \int_0^\infty d\rho\, F_n^a F_{n'}^a = \delta\left(n - n'\right) = \frac{dE_n}{dn}\delta\left(E_n - E_{n'}\right) = \frac{dE_n}{dn}\langle F_E | F_{E'} \rangle, \tag{A3}$$

which leads to $F_n^a = \sqrt{dE_n/dn} F_E$. Casting F_E into phase-amplitude form, after Milne [46],

$$F_E(k, \rho) \approx \sqrt{\frac{2m}{\pi \hbar^2}} \zeta(k) \sin [\beta(k, \rho)], \qquad (A4)$$

where the amplitude ζ and phase β satisfy

$$\left(\frac{d^2}{d\rho^2} + k^2(\rho, E) \right) \zeta - \frac{1}{\zeta^3} = 0, \qquad (A5)$$

$$\frac{d\zeta}{d\rho} - \frac{1}{\beta^2} = 0, \qquad (A6)$$

with the wave vector

$$k(\rho) = \sqrt{\frac{2m}{\hbar^2} (E - V(\rho))}. \qquad (A7)$$

The rapid oscillations of F_E in (A4) will have negligible effect on the integrals in Eqs. (A1) and (A2), where F_n^a is expressed in terms of F_E, except when ρ is near a turning point which is also a point of stationary phase. Away from a turning point, it is sufficient to use the

WKB approximations for the amplitude and phase:

$$\zeta(k) = \frac{1}{\sqrt{k(\rho, E)}}, \qquad (A8)$$

$$\beta(k, \rho) = \int_{\rho_t}^{\rho} d\rho' \, k(\rho', E) + \frac{\pi}{4}. \qquad (A9)$$

Near a turning point ρ_t, we expand the Milne phase to second order

$$\beta \approx b_0 + b_1(\rho - \rho_t) + \frac{b_2}{2}(\rho - \rho_t)^2 + ... \qquad (A10)$$

$$b_0 = \frac{\pi}{4}, \qquad (A11)$$

$$b_1 = \left. \frac{\partial \beta}{\partial \rho} \right|_{\rho = \rho_t} = k(\rho_t, E) = 0, \qquad (A12)$$

$$b_2 = \left. \frac{\partial^2 \beta}{\partial \rho^2} \right|_{\rho = \rho_t} = \left. \frac{\partial k}{\partial \rho} \right|_{\rho_t} = -\frac{m}{\hbar^2} \zeta^2 (k(\rho_t)) \left. \frac{\partial V}{\partial \rho} \right|_{\rho_t}. \qquad (A13)$$

Now, with

$$F_n^a = \sqrt{\frac{dE_n}{dn}} \sqrt{\frac{2m}{\pi \hbar^2}} \zeta(k) \sin [\beta(k, \rho)], \qquad (A14)$$

the integrand $F_n^a F^0$ is sharply localized around ρ_{1n}, the classical inner turning point. Thus,

$$\langle F_n^a | F^0 \rangle_\rho \approx F^0(\rho_{1n}) \int_0^\infty d\rho \, F_n^a(\rho) = F^0(\rho_{1n}) \sqrt{\frac{dE_n}{dn}} \sqrt{\frac{2m}{\pi \hbar^2}} \zeta(k(\rho_{1n})) \int_0^\infty d\rho \, \sin \left[b_0 + \frac{b_2}{2}(\rho - \rho_{1n})^2 \right]. \qquad (A15)$$

To evaluate the last integral, we use the formula

$$\int_0^\infty dx \cos(x^2) = \int_0^\infty dx \sin(x^2) = \frac{1}{2} \sqrt{\frac{\pi}{2}}. \qquad (A16)$$

Finally, we arrive at

$$\langle F_n^a | F^0 \rangle_\rho \approx F^0(\rho_{1n}) \sqrt{\frac{dE_n}{dn}} \sqrt{\frac{1}{|\partial V/\partial \rho|_{\rho_{1n}}}}. \qquad (A17)$$

The other overlap factor (A2) can be approximated in a similar fashion; it is given by

$$\langle F^\infty | F_n^a \rangle_\rho \approx (-1)^n F^\infty(\rho_{2n}) \sqrt{\frac{dE_n}{dn}} \sqrt{\frac{1}{|\partial V/\partial \rho|_{\rho_{2n}}}}, \qquad (A18)$$

where the $(-1)^n$ accounts for the sign of the rightmost amplitude around the outer turning point ρ_{2n} of the vibrational state if we set the leftmost amplitude around ρ_{1n} to be always positive as expressed in Eq. (A17).

Appendix B: Overlap between LOCV Hyperangular Wave Functions

To give a complete picture of the overlap between wave functions, the angular overlaps $\langle \Phi^a | \Phi^0 \rangle_\Omega$ and $\langle \Phi^\infty | \Phi^a \rangle_\Omega$ should also be considered. Real calculation involves $3N - 4$ dimensional integrals since this is the size of the hyperangular space. However, here, we only consider the one hyperangle, α, that describes the two-body interactions, and the large N case.

We start with a symmetrized Jastrow-type basis,

$$Y_\nu = \frac{\prod_{i<j} \phi_\nu(\rho; \alpha_{ij})}{\sqrt{\int d\Omega \prod_{i<j} \phi_\nu(\rho; \alpha_{ij})^2}}, \qquad (B1)$$

where α_{ij} is parametrically related to the coordinate distance between to particles, r_{ij} through $r_{ij} = \sqrt{2}\rho \sin \alpha_{ij}$; the function ϕ_ν satisfies the Bethe-Peierls boundary condition which describes what happens when two particles are close to each other. The other boundary condition is set by treating $|\phi_\nu|^2$ as a pair correlation function such that if two atoms are more than distance

$r_d = \sqrt{2}\rho \sin\alpha_d$ apart, then they become uncorrelated or $|\phi(\alpha_{ij} \geq \alpha_d)|^2 = 1$. Therefore, within a region bounded by α_d, there is on the average only one other atom (out of $N-1$) which can be seen by a fixed atom, or

$$\frac{4\pi \int_0^{\alpha_d} d\Omega_\alpha \int d\Omega_{N-2} \prod_{i<j} |\phi_\nu(\rho;\alpha_{ij})|^2}{\int d\Omega_{N-1} \prod_{i<j} |\phi_\nu(\rho;\alpha_{ij})|^2} = \frac{1}{N-1}, \quad \text{(B2)}$$

where $d\Omega = d\Omega_{N-1} = 4\pi d\Omega_\alpha d\Omega_{N-2}$, and $d\Omega_\alpha = \sin^2\alpha \cos^{3N-7}\alpha\, d\alpha$. If $\alpha_d = \pi/2$, then the right side of (B2) should be one. The full form of the pair correlation function g_2 can be written as

$$g_2(\alpha) = \left(4\pi \int_0^{\pi/2} d\Omega_\alpha\right) \frac{\int d\Omega_{N-2} \prod_{i<j} |\phi_\nu(\rho;\alpha_{ij})|^2}{\int d\Omega_{N-1} \prod_{i<j} |\phi_\nu(\rho;\alpha_{ij})|^2}, \quad \text{(B3)}$$

which is hard to evaluate. To lowest order, however, it is approximated to be $g_2(\alpha) = |\phi_\nu(\alpha)|^2$. This whole procedure outlined above describes a lowest order constraint variational (LOCV) method in hyperspherical coordinates; details can be found in Ref.[10]. Given ρ and the scattering length a, one can then find α_d and ϕ_v. The angle α_d becomes extremely small as N increases. Hence $\phi(\rho;\alpha_{ij})$ is unity in large region of α_{ij} - this is an approximation that leads to $g_2(\alpha) = |\phi_\nu(\alpha)|^2$.

In the following derivations, we will also treat all the pair wave functions $\phi(\rho,\alpha_{i'j'})$ equivalent to unity, except one pair namely, $\phi(\rho,\alpha_{12}) = \phi(\rho,\alpha)$. So,

$$\langle \Phi^a|\Phi^0\rangle_\Omega \approx \mathcal{N}_0 \mathcal{N}_a \int_0^{\pi/2} d\alpha\, \alpha^2 \phi^a(\rho_{1n};\alpha)\phi^0(\rho_{1n};\alpha) \quad \text{(B4)}$$

$$\langle \Phi^\infty|\Phi^a\rangle_\Omega \approx \mathcal{N}_\infty \mathcal{N}_a \int_0^{\pi/2} d\alpha\, \alpha^2 \phi^\infty(\rho_{2n};\alpha)\phi^a(\rho_{2n};\alpha) \quad \text{(B5)}$$

where the $\mathcal{N}$'s are some normalization constants so that $\langle \Phi^0|\Phi^0\rangle_\Omega = 1$, $\langle \Phi^a|\Phi^a\rangle_\Omega = 1$, and $\langle \Phi^\infty|\Phi^\infty\rangle_\Omega = 1$, and [10]

$$\phi^0(\rho;\alpha) = 1 \quad \text{(B6)}$$

$$\phi^a(\rho;\alpha) \approx A\left(1 - \frac{a}{\sqrt{2}\rho}\frac{1}{\alpha}\right), \quad \text{if } \alpha < \alpha_a \quad \text{(B7)}$$

$$\phi^\infty(\rho;\alpha) = B\frac{\cos\left(\sqrt{6N\nu_\infty}\alpha\right)}{\alpha} \quad \text{if } \alpha < \alpha_\infty, \quad \text{(B8)}$$

$$v_\infty = c_0 N^{2/3} \quad \text{(B9)}$$

The wave functions ϕ^a and ϕ^∞ identically approach unity for $\alpha > \alpha_a$ and $\alpha > \alpha_\infty$, which are given by

$$\alpha_a \approx \left(\frac{\pi}{6}\right)^{1/6} N^{-5/6} \quad \text{(B10)}$$

$$\alpha_\infty \approx \left(\frac{2\pi}{27}\right)^{1/6} N^{-5/6}. \quad \text{(B11)}$$

Note that α_a and α_∞ are extremely small for large N so that the integrals in Eqs. (B4) and (B5) are over large part of the α-space where ϕ^a and ϕ^∞ are unity. The constants A and B are determined from the continuity boundary condition at α_a and α_∞:

$$A \approx 1 + \frac{a}{\sqrt{2}\rho}\frac{1}{\alpha_a}, \quad \text{(B12)}$$

$$B = \frac{\alpha_\infty}{c_1} = \frac{1}{c_1}\left(\frac{2\pi}{27}\right)^{1/6} N^{-5/6}, \quad \text{(B13)}$$

$$c_1 = \cos\left(\sqrt{6N\nu_\infty}\alpha_\infty\right) \approx -0.942. \quad \text{(B14)}$$

We then find

$$\mathcal{N}_0 = \sqrt{\frac{24}{\pi^3}}, \quad \text{(B15)}$$

$$\mathcal{N}_a \approx \sqrt{\frac{24}{\pi^3}}\left[1 + \frac{2\sqrt{2}}{\pi^3}\frac{a}{\rho}\alpha_a^2 + \frac{4}{\pi^3}\left(\frac{a}{\rho}\right)^2\alpha_a + ...\right], \quad \text{(B16)}$$

$$\mathcal{N}_\infty \approx \sqrt{\frac{24}{\pi^3}}\left[1 - \frac{12}{\pi^3}\gamma N^{-5/2} + ...\right], \quad \text{(B17)}$$

$$\gamma = \frac{c_2}{2c_1\sqrt{6c_0}}\left(\frac{2\pi}{27}\right)^{1/3} + \frac{1}{2c_1^2} - \frac{1}{3} \approx 0.1997 \quad \text{(B18)}$$

$$c_2 = \sin\left(\sqrt{6N\nu_\infty}\alpha_\infty\right) \approx 0.336. \quad \text{(B19)}$$

Finally, after a series of algebraic steps and careful bookkeeping of N-scaling of the relevant parameters, we find

$$\langle \phi^0|\phi^a(\rho_{1n})\rangle_\alpha \approx 1 - \frac{2}{\pi^3}\left(\frac{a}{\rho_{1n}}\right)^2\alpha_a, \quad \text{(B20)}$$

$$\langle \phi^\infty|\phi^a(\rho_{2n})\rangle_\alpha \approx 1 - 0.151 N^{-5/2}, \quad \text{(B21)}$$

which are our approximations for $\langle \Phi^a|\Phi^0\rangle_\Omega$ and $\langle \Phi^\infty|\Phi^a\rangle_\Omega$, respectively. For large N, these quantities are both essentially equal to one.

Appendix C: The Transition Amplitude

We evaluate the transition amplitude at $t = t_m \approx \pi/(2\omega)$ at large N. In terms of the Franck-Condon factors derived in Appendix A, we write the transition amplitude as

$$\langle \infty, 0 | \Psi^a(t_m) \rangle \approx \sum_{n=0}^{\infty} (-1)^n F^0(\rho_{1n}) F^{\infty}(\rho_{2n}) \frac{dE_n}{dn} \sqrt{\frac{1}{|\partial V/\partial \rho|_{\rho_{1n}}}} \sqrt{\frac{1}{|\partial V/\partial \rho|_{\rho_{2n}}}} e^{i\omega_n t_m}, \tag{C1}$$

with $\omega_n \approx (2 + \Delta_n) n\omega$, where $\Delta_n < 1$ ($\Delta_n \ll 1$ for small a). Thus,

$$(-1)^n e^{i\omega_n t_m} \approx e^{i(n\pi + \omega_n t_m)} = e^{i2n\pi} = 1. \tag{C2}$$

Also, using Eqs. (31) and (32),

$$\left. \frac{\partial V}{\partial \rho} \right|_{\rho_{1n}} \approx -3 \left(\frac{m}{\hbar^2 d_0 N^{7/2} a} \right)^{1/3} E_n^{4/3}, \tag{C3}$$

$$\left. \frac{\partial V}{\partial \rho} \right|_{\rho_{2n}} \approx \sqrt{2m\omega^2 E_n}. \tag{C4}$$

Converting the discrete sum into an integral over energy, $\sum_n \to \int dE$, and using the form of F^0 and F^{∞} in Eqs. (27) and (28), and noting that the resulting integrand is strongly peaked at $E^* \approx \sqrt{3c_0} N^{4/3} \hbar\omega/2 \approx 1.26 N^{4/3} \hbar\omega$ (see Eqs. (34) and (23)), we get

$$|\langle \infty, 0 | \Psi^a(t_m) \rangle| \approx \frac{2(2d_0)^{1/6}}{\sqrt{3\pi}(\sqrt{3c_0})^{11/12}} \left(\frac{a}{a_{ho}} \right)^{1/6} N^{-23/36} \frac{1}{\hbar\omega} \int_0^{\infty} dE \exp \left[-\frac{(\rho_1(E) - \rho^0)^2}{a_{ho}^2} \right] \exp \left[-\frac{(\rho_2(E) - \rho^{\infty})^2}{a_{ho}^2} \right], \tag{C5}$$

with $\rho_1 \approx (\frac{\hbar^2}{m} d_0 N^{7/2} a)^{1/3} E^{-1/3}$ and $\rho_2 \approx \sqrt{2E/(m\omega^2)}$ from Eqs. (31) and (32). Now, $F^{\infty}(\rho_2(E))$ is a peaky function of E. We can then use the saddle point approximation to solve the integral in Eq. (C5):

$$\int_0^{\infty} dE \exp \left[-\frac{(\rho_1(E) - \rho^0)^2}{a_{ho}^2} \right] \exp \left[-\frac{(\rho_2(E) - \rho^{\infty})^2}{a_{ho}^2} \right] = \hbar\omega\sqrt{\pi} \frac{\rho^{\infty}}{a_{ho}} \exp \left[-\frac{\left(\left(2d_0 N^{7/2} a_{ho}^4 \frac{a}{\rho^{\infty 2}} \right)^{1/3} - \rho_0 \right)^2}{a_{ho}^2} \right]. \tag{C6}$$

Finally, expressing ρ^0 and ρ^{∞} in terms of N,

$$|\langle \infty, 0 | \Psi^a(t_m) \rangle| \approx \frac{2(2d_0)^{1/6}}{(3c_0)^{5/24}\sqrt{3}} N^{1/36} \left(\frac{a}{a_{ho}} \right)^{1/6} \exp \left[-\left(\left(\frac{2d_0}{\sqrt{3c_0}} \right)^{1/3} N^{13/18} \left(\frac{a}{a_{ho}} \right)^{1/3} - \sqrt{\frac{3N}{2}} \right)^2 \right]. \tag{C7}$$

[1] P. Makotyn, C. E. Klauss, D. L. Goldberger, E. A. Cornell, and D. S. Jin, Nat. Phys. **10**, 116 (2014).

[2] C. E. Klauss, X. Xie, C. Lopez-Abadia, J. P. D'Incao, Z. Hadzibabic, D. S. Jin, and E. A. Cornell, Phys. Rev.

Lett. **119**, 143401 (2017).

[3] C. Eigen, J. A. P. Glidden, R. Lopes, N. Navon, Z. Hadzibabic, and R. P. Smith, Phys. Rev. Lett. **119**, 250404 (2017).

[4] R. J. Fletcher, R. Lopes, J. Man, N. Navon, R. P. Smith, M. W. Zwierlein, and Z. Hadzibabic, Science **355**, 377 (2017).

[5] R. J. Fletcher, A. L. Gaunt, N. Navon, R. P. Smith and Z. Hadzibabic, Phys. Rev. Lett. **111**, 125303 (2013).

[6] J. L. Song and F. Zhou, Phys. Rev. Lett. **103**, 025302 (2009).

[7] Y. L. Lee and Y. W. Lee, Phys. Rev. A **81**, 063613 (2010).

[8] F. Zhou and M. S. Mashayekhi, Ann. Phys. **328**, 83 (2013).

[9] Y. Ding and C. H. Greene, Phys. Rev. A **95**, 053602 (2017).

[10] M. W. C. Sze, A. G. Sykes, D. Blume, and J. L. Bohn Phys. Rev. A **97**, 033608 (2018).

[11] S. Cowell, H. Heiselberg, I. E. Mazets, J. Morales, V. R. Pandharipande, and C. J. Pethick, Phys. Rev. Lett. **88**, 210403 (2002).

[12] D. Borzov, M. S. Mashayekhi, S. Zhang, J.-L. Song and F. Zhou, Phys. Rev. A **85**, 023620 (2012).

[13] J. M. Diederix, T. C. F. van Heijst, and H. T. C. Stoof, Phys. Rev. A **84**, 033618 (2011).

[14] X. Yin and L. Radzihovsky, Phys. Rev. A **88**, 063611 (2013).

[15] H. T. C. Stoof and J. J. R. M. van Heugten, J. Low Temp. Phys. **174**, 159 (2014).

[16] M. Rossi, L. Salasnich, F. Ancilotto and F. Toigo, Phys. Rev. A **89**, 041602(R) (2014).

[17] A. G. Sykes, J. P. Corson, J. P. D'Incao, A. P. Koller, C. H. Greene, A. M. Rey, K. R. A. Hazzard, and J. L. Bohn, Phys. Rev. A **89**, 021601 (2014).

[18] D. H. Smith, E. Braaten, D. Kang and L. Platter, Phys. Rev. Lett. **112**, 110402 (2014).

[19] C. Eigen, J. A. P. Glidden, R. Lopes, E. A. Cornell, R. P. Smith, and Z. Hadzibabic, Nature **563**, 221 (2018).

[20] J. P. D'Incao, J. Wang, and V. E. Colussi, Phys. Rev. Lett. **121**, 023401 (2018).

[21] P. F. Bedaque, E. Braaten, and H.-W. Hammer, Phys. Rev. Lett. **85**, 908 (2000).

[22] E. Braaten and H.-W. Hammer, Physics Reports **428**, 259 (2006).

[23] J. von Stecher and C. H. Greene, Phys. Rev. A **75**, 022716 (2007).

[24] Interestingly, the opposite technique was applied in the JILA experiment, jumping to a smaller scattering length to create a denser condensate, to explore density effects. See C. E. Klauss, Doctoral dissertation, University of Colorado Boulder (2017).

[25] J. L. Bohn, B. D. Esry, and C. H. Greene, Phys. Rev. A **58**, 584 (1998).

[26] B. M. Garraway and K.-A. Suominen, Contemporary Physics **43**, 97 (2002).

[27] O. Sørensen, D. V. Fedorov, and A. S. Jensen, Phys. Rev. A **66**, 032507 (2002).

[28] T. K. Das and B. Chakrabarti, Phys. Rev. A **70**, 063601 (2004).

[29] T. K. Das, S. Canuto, A. Kundu, and B. Chakrabarti, Phys. Rev. A **75**, 042705 (2007).

[30] B. Chakrabarti and T. K. Das, Phys. Rev. A **78**, 063608 (2008).

[31] M. L. Lekala, B. Chakrabarti, G. J. Rampho, T. K. Das, S. A. Sofianos, and R. M. Adam, Phys. Rev. A **89**, 023624 (2014).

[32] O. Sørensen, D. V. Fedorov, and A. S. Jensen, Phys. Rev. A **68**, 063618 (2003).

[33] O. Sørensen, D. V. Fedorov, and A. S. Jensen, J. Phys. B **37**, 93 (2004).

[34] T. Sogo, O. Sørensen, A. S. Jensen, and D. V. Fedorov, J. Phys. B **38**, 1051 (2005).

[35] Yu. F. Smirnov and K. V. Shitikova, Sov. J. Part. Nucl. **8**, 344 (1977).

[36] Y. Castin, C. R. Physique **5**, 407 (2004).

[37] F. Werner and Y. Castin, Phys. Rev. A **74**, 053604 (2006).

[38] E. U. Condon, Phys. Rev. **32**, 858 (1928).

[39] J. G. Winans and E. C. G. Stückelberg, Proc. Nat. Acad. Sci. **857**, 1928).

[40] K.-A. Suominen, J. Phys. B **29**, 5981, (1996).

[41] J. Weiner, V. Bagnato, S. Zilio, and P. S. Julienne, Rev. Mod. Phys. **71**, 1, (1999).

[42] J. L. Bohn and P. S. Julienne, Phys. Rev. A **60**, 414 (1999).

[43] C. Boisseau, E. Audouard, J. Vigue, and P. S. Julienne, Phys. Rev. A **62**, 052705 (2000).

[44] P. S. Julienne, J. Res. Natl. Inst. Stand. Technol. **101**, 487, (1996).

[45] A. Jablonski, Phys. Rev. **68**, 78 (1945).

[46] W. E. Milne, Phys. Rev. **35**, 863 (1930); F. Robicheaux, U. Fano, M. Cavagnero, and D. A. Harmin, Phys. Rev. A **35**, 3619 (1987).